Crystal Structure of Homoserine Transacetylase from *Haemophilus influenzae* Reveals a New Family of α/β-Hydrolases[†,‡]

I. Ahmad Mirza,[§] Ishac Nazi,[||] Magdalena Korczynska,[§] Gerard D. Wright,[||] and Albert M. Berghuis*[,§]

Department of Biochemistry and Department of Microbiology and Immunology, McGill University, Montreal, Quebec, Canada H3A 1A4, and Antimicrobial Research Centre and Department of Biochemistry and Biomedical Sciences, McMaster University, Hamilton, Ontario, Canada L8N 3Z5

Received September 27, 2005

ABSTRACT: Homoserine transacetylase catalyzes one of the required steps in the biosynthesis of methionine in fungi and several bacteria. We have determined the crystal structure of homoserine transacetylase from *Haemophilus influenzae* to a resolution of 1.65 Å. The structure identifies this enzyme to be a member of the α/β-hydrolase structural superfamily. The active site of the enzyme is located near the end of a deep tunnel formed by the juxtaposition of two domains and incorporates a catalytic triad involving Ser143, His337, and Asp304. A structural basis is given for the observed double displacement kinetic mechanism of homoserine transacetylase. Furthermore, the properties of the tunnel provide a rationale for how homoserine transacetylase catalyzes a transferase reaction vs hydrolysis, despite extensive similarity in active site architecture to hydrolytic enzymes.

The aspartate pathway is one of the critical amino acid biosynthetic pathways found in all kingdoms except animals (*1*). In bacteria, plants, and fungi this pathway converts Asp into the essential amino acids Ile, Met, and Thr. Furthermore, in bacteria the aspartate pathway also forms the starting point for the synthesis of Lys (*2*). In brief, metabolic processing of Asp is initiated via phosphorylation of the C4 carboxyl, followed by two successive two-electron reduction steps generating the corresponding C4-alcohol. The resulting product, homoserine, is then situated at a key metabolic branch point where it can be either phosphorylated and subsequently further converted into Thr and Ile or acylated, directing it toward Met biosynthesis. In fungi and many clinically important bacterial species (e.g., *Pseudomonas aeruginosa*, *Mycobacterium tuberculosis*, and *Haemophilus influenzae*) the enzyme that commits homoserine toward Met biosynthesis is homoserine transacetylase (HTA).

The critical nature of the aspartate pathway is not only the result of the necessity of maintaining sufficient pools of amino acids for protein synthesis but it also affects numerous other metabolic processes as Met is the precursor to the essential biological methyl donor, *S*-adenosylmethionine (*3*). As a consequence of this critical biochemical role and the absence of a homologous pathway in humans, enzymes of the aspartate pathway have been considered as potential drug targets for antimicrobial drug development. The viability of exploiting these enzymes as drug targets has been demonstrated in the antifungal/antimycobacterial compound 5-hydroxy-4-oxonorvaline, which targets the enzyme upstream of HTA, homoserine dehydrogenase (*4*).

Given the potential relevance of enzymes of the aspartate pathway in antimicrobial drug discovery, it is not surprising that they have been the subject of extensive studies including structural characterization. For example, the pathway has been probed by genetic tools to identify factors affecting its flux (*5*); inhibitors have been identified through high-throughput screening methods and other approaches (*4*, *6*, *7*); and enzymological studies have been reported for all of the enzymes that make up the aspartate pathway (*2*). Crystal structures have been determined for four of the enzymes involved in the aspartate pathway, i.e., the two enzymes preceding HTA in the pathway, aspartate semialdehyde dehydrogenase (*8*) and homoserine dehydrogenase (*9*), and the two enzymes that follow HTA toward Met synthesis, cystathione γ-synthase (*10*) and cystathionine β-lyase (*11*).

HTA has thus far resisted structural characterization but has been kinetically characterized. Blanchard and co-workers have reported studies for HTA from *H. influenzae*, and we have studied the *Schizosaccharomyces pombe* homologue (*12*, *13*). These studies show that HTA catalyzes the transfer of the acetyl group from coenzyme A to homoserine employing a double displacement (ping-pong) mechanism, involving an acyl-enzyme intermediate. Here we present the crystal structure of HTA from *H. influenza* to 1.65 Å resolution and discuss its mechanistic implications.

EXPERIMENTAL PROCEDURES

Cloning of HTA from H. influenzae. The *met2* gene encoding HTA was amplified from *H. influenza*e genomic DNA using the oligonucleotides ML662, 5′-GGGAATTC-CATATGTCTGTGCAAAATGTAGTG, and ML663, 5′-

[†] This work was supported by the Canadian Institutes of Health Research (Grant MOP-77824), Crompton Corp./Cie, and by Canada Research Chairs in Structural Biology (to A.M.B.) and Antibiotic Biochemistry (to G.D.W.).

[‡] Atomic coordinates for HTA have been deposited in the Protein Data Bank (accession number 2B61).

* Corresponding author: phone, (514) 398-8795; fax, (514) 398-2036; e-mail, albert.berghuis@mcgill.ca.

[§] McGill University.

[||] McMaster University.

10.1021/bi051951y CCC: $30.25
Published on Web 11/05/2005

TCCCCCCGGGAAGCTTTTAATTACCTGCCAAACCATC. The amplicon was cloned into the pET28 vector (Novagen) at the *Nde*I and *Hin*dIII restriction enzyme sites using standard techniques, and the DNA sequence was verified. The resulting plasmid was transformed into *Escherichia coli* B834 DE3 competent cells, allowing for the expression of HTA with an N-terminal hexahistidine tag.

Expression and Purification of Selenomethionine-Labeled HTA. Transformed cells were grown at 37 °C in 2 L of M9 minimal media supplemented with selenomethionine to an OD_{600nm} of 1.0, at which time induction was achieved by the addition of isopropyl β-D-thiogalactopyranoside to 1 mM. Cells were then grown for an additional 9 h, harvested by centrifugation at 6000*g*, and resuspended in 30 mL of 50 mM HEPES, pH 7.5, 500 mM NaCl, and 20 mM imidazole. Lysis was performed by sonication and cleared by centrifugation at 21000*g* for 45 min. The supernatant was subsequently passaged through a 0.22 μm filter and applied onto a 5 mL HiTrap Chelating HP column (Amersham). Protein was eluted by using an increasing gradient of imidazole to a final concentration of 200 mM. Fractions showing absorbance at 280 nm were analyzed by SDS−polyacrylamide gel electrophoresis, and fractions containing HTA were pooled. After the pooled fractions were concentrated, the sample was applied to a Sephacryl S200 sizing column and eluted using 50 mM HEPES, pH 7.5, 500 mM NaCl, and 20 mM imidazole. Fractions corresponding to single bands on a Coomassie-stained polyacrylamide gel were subsequently assayed for enzyme activity (*12*, *13*), pooled, and concentrated to 10 mg/mL.

Crystallization, Data Collection, and Data Processing. Crystals of HTA were grown by the hanging drop vapor diffusion method using a 1:1 protein to well solution ratio for a total drop size of 4 μL. Diffraction quality crystals were obtained in 1−2 days when using 20% PEG 8000 and 100 mM HEPES, pH 7.5, as the well solution. In preparation for data collection crystals were briefly soaked in PEG 200 and flash frozen. Diffraction data from two crystals, collected at one and two different wavelengths, were acquired at the X29 and X8C beamlines of the National Synchrotron Light Source, Brookhaven National Laboratories, Upton, NY, respectively. Data were processed using the HKL2000 software suite (*14*). Details of data collection statistics are provided in Table 1.

Structure Determination and Refinement. Diffraction data originating from the two crystals were separately used for structure determination, employing Solve/Resolve (*15*) followed by automated model building with ARP/wARP (*16*). In both cases, Solve readily identified eight out of a possible nine selenium sites present in the asymmetric unit. The two independent models resulting from this automated procedure revealed remarkable agreement with an rmsd of 0.121 Å for 341 Cα atoms (94% complete model; Figure 1). Given the higher (1.65 Å) resolution of the data measured at the X29 beamline, this model was further refined using refmac (*17*). The final model of HTA consists of residues 2−358 and 425 solvent molecules but excludes the N-terminal hexa-His tag as no density for this peptide was observed. Phasing and refinement statistics are provided in Table 1.

Table 1: Data Collection, Data Processing, Phasing, and Refinement Statistics[a]

Data Collection			
X-ray source	BNL-X29	BNL-X8C	
space group	$P3_121$	$P3_121$	
cell dimensions (Å)	$a = b = 85.3$, $c = 120.3$	$a = b = 85.8$, $c = 120.8$	
wavelength (Å)	0.9788	0.9800	0.9184
Data Processing			
resolution (Å)	50.0−1.65 (1.71−1.65)	50.0−2.19 (2.27−2.19)	50.0−2.06 (2.13−2.06)
completeness (%)	98.8 (98.6)	97.5 (94.8)	99.8 (99.3)
R_{merge} (%)	7.1 (32.9)	9.7 (16.5)	7.1 (21.9)
I/σ	10.8 (4.0)	9.3 (6.3)	12.8 (5.1)
Phasing			
FOM (prior den. mod.)	0.34	0.48	
FOM (post den. mod.)	0.75	0.77	
Refinement			
unique reflections	57586		
R_{factor} (%)	16.4		
R_{free} (%)	18.7		
rmsd bonds (Å)	0.010		
rmsd angles (deg)	1.155		

[a] Values for the highest resolution shell are shown in parentheses.

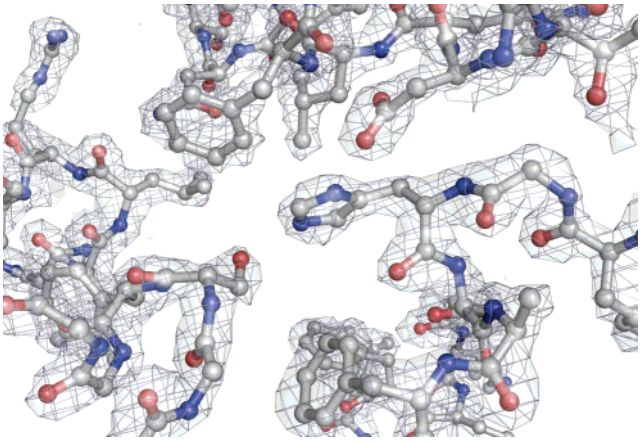

FIGURE 1: Electron density map obtained immediately following density modification and automated model building with ARP/wARP. The map is contoured at 1σ. Superposed on the electron density map is the final refined model of HTA. The portion of the molecule shown includes residues Ser143, Asp304, and His337. This figure and similar following figures were prepared using PyMOL (*27*).

RESULTS AND DISCUSSION

Overall Fold of HTA. The structure of HTA reveals a two-domain organization, where one domain consists of residues 1−167 and 281−358 and the second domain is composed of residues 173−276 (Figure 2a,b). The first domain consists of an eight-stranded strongly twisted β-sheet, which is predominantly parallel in topology. Connectivity of this β-sheet is achieved by two flanking α-helices parallel to the sheet on one side and three helices on the opposite face. The second domain is inserted between β-strand 6 and helix D and is composed of five α-helices. The orientation of this domain is perpendicular to the β-sheet and forms a canopy over the first domain. The intervening residues between the two domains (residues 168−172 and 277−281) do not display any secondary structure.

The group of Dr. Blanchard has suggested that HTA from *H. influenzae* exists physiologically as a dimer (*12*). The crystal structure determined here has only one HTA molecule per asymmetric unit. However, examination of crystal

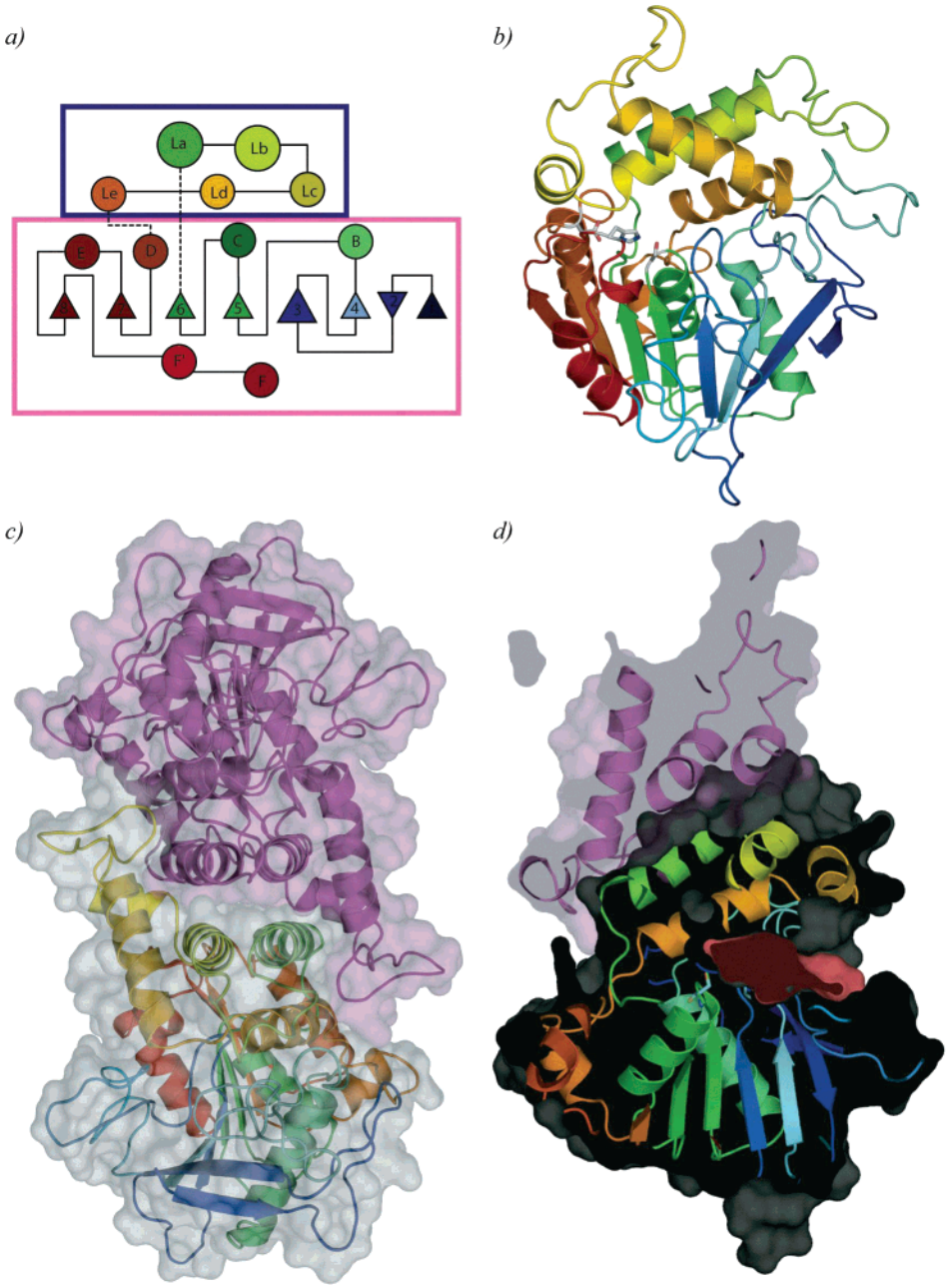

FIGURE 2: Structure of HTA from *H. influenzae*. (a) TOPS diagram of HTA in which the two-domain architecture of enzyme is highlighted by boxes (*28*). The secondary structure nomenclature follows the canonical labeling scheme used for α/*β*-hydrolase enzymes. (b) Cartoon representation of HTA colored according to (a). (c) Quaternary structure of HTA. (d) Cross section of the enzyme illustrating the size and depth of the active site tunnel.

packing contacts reveals that two HTA molecules can form a physiological dimer species through interactions between the two all-α-helical domains (Figure 2c). Helices La and Lb from one monomer are found to interact in an antiparallel orientation with the complementary helices of the adjacent molecule. Together they form a classical four-helix bundle arrangement in which the core is completely hydrophobic. Additionally, helices Lc and Ld perpendicularly flank the four-helix bundle, thereby further strengthening dimeric interactions by providing both hydrogen bonds and van der Waals contacts. As a result, the two HTA monomers form an arrangement resembling a handshake. The total extent of the dimer interface is 2200 Å^2 (per monomer) and is predominantly hydrophobic in character, in full agreement with what has been observed for physiologically stable dimers (*18*). Note that the dimer interactions are limited to residues from one domain, leaving the possibility of domain movement within one HTA monomer.

The most striking feature of the molecular surface of HTA is a deep tunnel formed by the juxtaposition of the two domains (Figure 2d). The tunnel is cylindrically shaped with a length of ∼14 Å and a diameter of ∼7 Å. The overall volume of the tunnel is approximately 650 Å^3. The residues lining the wall of the tunnel are predominantly polar and include residues Thr50, Asp52, Arg61, Ser143, Arg212, Tyr219, Tyr294, His337, and Asp338. Intriguingly, Ser143 is the only residue in HTA which displays strained ϕ/ψ angles despite having very well defined density, suggesting its strained conformation is important for function (Figure 1).

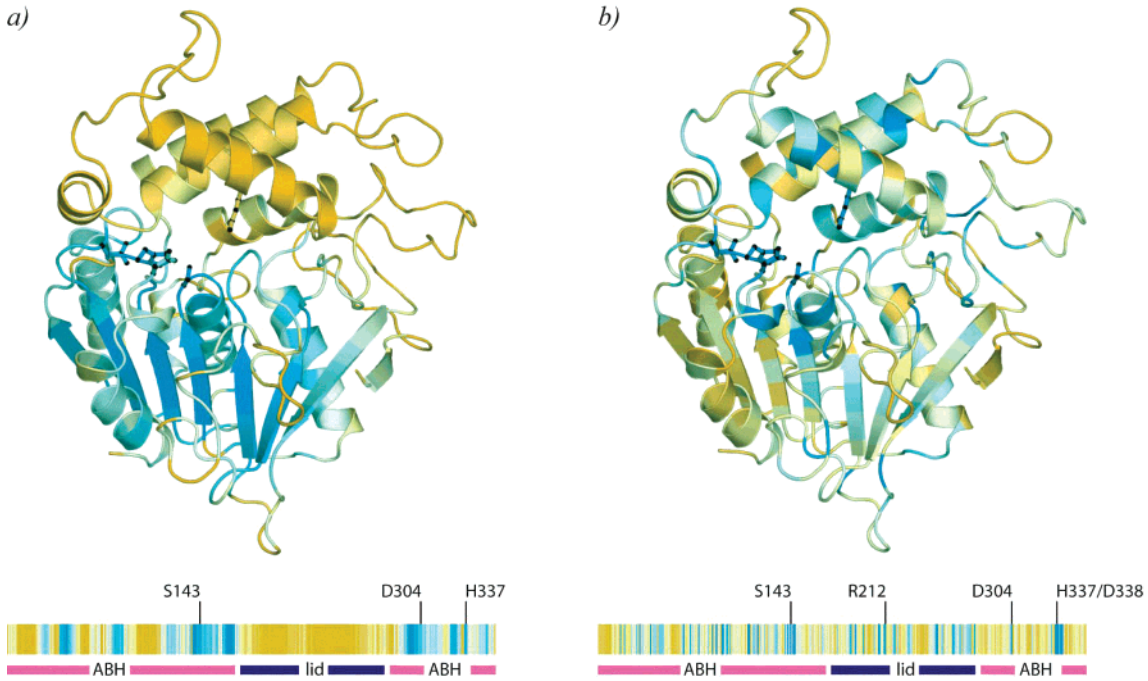

FIGURE 3: Comparison of HTA with members of the α/β-hydrolase superfamily and other HTA enzymes. (a) rmsd comparison of HTA vs 33 diverse family members from SCOP database (*29*). Residues that are structurally conserved are colored blue, and those that possess no structurally equivalent residues in other α/β-hydrolase superfamily members are colored yellow. The scoring results are presented both as a cartoon representation and as a fingerprint (*30*). Structural alignments were carried out using Lsqman (*31*). (b) Similar to (a) except that here sequence similarity among 24 unique HTA sequences in GenBank is mapped onto the structure. Unique sequences used in this comparison were obtained using Blastp. Alignments were carried out with ClustalX (*32*), and scoring of residues was assessed using a Gonnet 350 matrix (*33*).

HTA Is a Member of the α/β-Hydrolase Superfamily. VAST analysis (*19*) reveals that the second all-α-helical domain possesses a unique fold. However, the first β-sheet-containing domain displays a fold which identifies HTA as a member of the α/β-hydrolase structural superfamily (Figure 3a). The α/β-hydrolase superfamily has been well studied for over 15 years (*20*). The canonical fold consists of an eight-stranded mainly parallel β-sheet, in which the second strand is oriented in the antiparallel direction, surrounded by a total of six α-helices (*21*). Significant amino acid sequence similarity among the various members of this superfamily is effectively nonexistent, implying substantial evolutionary divergence (*22*). This divergence is also reflected in the plethora of chemical transformations catalyzed by α/β-hydrolase superfamily members. The following catalytic activities have been observed in members of this superfamily: hydrolase, thioesterase, haloperoxidase, dehalogenase, and C−C bond breaking (*23*). HTA's β-sheet-containing domain, hereafter referred to as the α/β-hydrolase (ABH) domain, is structurally most similar to a putative serine hydrolase (Ydr428C) from *Saccharomyces cerevisiae* (PDB code 1VKH), with an rmsd of 3.9 Å for 204 aligned residues. When the second domain of HTA, hereafter referred to as the lid domain, is included in the structural comparison, proline iminopeptidase from *Xanthomonas campestris* (PDB code 1AZW) is identified as the nearest structural homologue in the current Protein Data Bank (rmsd of 3.4 Å for 259 residues). The ABH domain differs most significantly from the canonical α/β-hydrolase fold in the absence of α-helix A, which is normally located between β-strands 2 and 3 but which is replaced in HTA by a loop that lacks secondary structure.

It is somewhat unexpected that HTA is a member of the α/β-hydrolase superfamily. BLAST search of the amino acid sequence against the current Protein Data Bank does not reveal any significant hits. The structure-based sequence alignments of HTA to its nearest structural neighbors also show percent sequence identity of 10% or less. However, bioinformatics analysis using the Conserved Domain Database does predict HTA to be a member of the α/β-hydrolase superfamily (*24*). As a result, several groups including ours have speculated that HTA may possess the α/β-hydrolase fold (*13*, *25*, *26*).

Structural Basis for the Catalytic Mechanism of HTA. Comparison of all HTA sequence data presently available indicates that the average pairwise percent identity is ∼30−40% (Figure 3b). Specifically, the following residues that are adjacent to the tunnel are absolutely conserved: Ser143, Arg212, Asp304, His337, and Asp338. Furthermore, some of these residues (Ser143, Asp304, and His337) are strongly, though not absolutely, conserved among α/β-hydrolase superfamily members. Note that HTA's from some organisms are significantly longer than the *H. influenza* enzyme, possessing inserts between helices Lc and Ld or Le and D, which are unlikely to impact activity. Previous kinetic studies of HTA from *H. influenzae* and *S. pombe* show that HTA-catalyzed acetylation of homoserine follows a double displacement (ping-pong) mechanism where acetyl-CoA donates the acetyl group to a nucleophilic residue, thus forming an initial acyl-enzyme intermediate, followed by a transfer of the acetyl group to homoserine (*12*, *13*). Mutagenesis studies with the *S. pombe* enzyme have provided additional information on the nature of the nucleophilic residue and possible mechanism of activating the nucleophile; specifically, Ser143

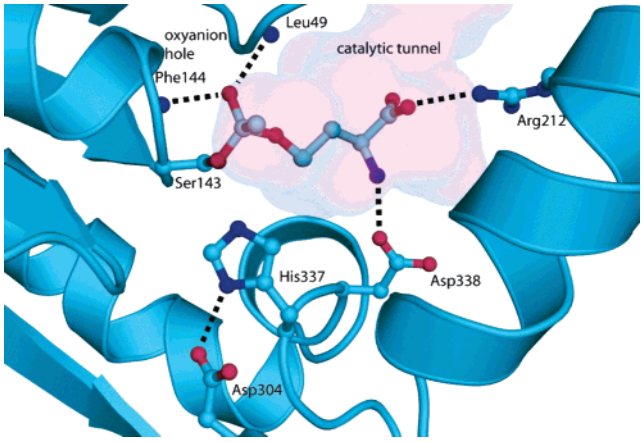

FIGURE 4: Schematic representation of the tunnel and active site architecture. Shown is the proposed transition state geometry for acyl transfer to homoserine, indicating positioning of the substrate by Arg212 and Asp338.

was identified as the catalytic nucleophile, and residues equivalent to *H. influenzae* His337 and Asp304 were predicted to complete a catalytic triad for acyl transfer (*13*). By incorporating these results with the structural data presented here and exploiting similarities with other enzymes of the α/β-hydrolase superfamily, a detailed catalytic mechanism can be proposed.

The structure of HTA reveals that the conserved residue Ser143 is in a strained conformation and ideally positioned in the tunnel to function as the nucleophilic residue that accepts the acetyl group from acetyl-CoA. Adjacent to Ser143 is His337, which is in hydrogen-bonding distance of the solvent-exposed Ser143 hydroxyl through its Nϵ (2.60 Å). Furthermore, His337 is also in hydrogen-bonding distance of the side-chain moiety of Asp304 through Nδ (2.75 Å). This constellation is reminiscent of the catalytic triad in, for example, serine proteases and will force Ser143 to be in an activated state so as to favor nucleophilic attack on this residue (Figure 1). Entrance of the first substrate acetyl-CoA into the active site results in nucleophilic attack on the thioester bond of acetyl-CoA. Formation of the predicted tetrahedral transition state can be stabilized via an oxyanion hole formed by the backbone amide nitrogens of Leu49 and Phe144. Phe144 is situated at the N-terminus of helix C, which contributes additional positive charge via helical dipole interactions. Collapse of the tetrahedral transition state precipitates release of CoASH, resulting in an acylated Ser143: the acyl-enzyme intermediate. Next, entrance of the alcohol homoserine affects a reverse of the previous reaction with transfer of the acetyl group back from the enzyme onto homoserine via a second tetrahedral transition state again stabilized by the same oxyanion hole (Figure 4).

The reaction mechanism presented is analogous to what has been previously described for hydrolase and thioesterase members of the α/β-hydrolase superfamily. However, there is one significant difference: the reaction catalyzed is not hydrolytic; i.e., following acyl-enzyme formation, the acyl moiety is not transferred to a water molecule but instead to a specific second substrate, in this case homoserine. This difference raises an intriguing question: namely, how does HTA prevent transfer of the acetyl group from the acyl-enzyme intermediate to a water molecule but instead favors transfer to homoserine? To fully address this question, structural information on the acyl-enzyme intermediate and on the homoserine binding site will be required. However, the structure presented here provides some insights. Two possible strategies can be conceived by which HTA could circumvent acting as a thioesterase: (i) excluding water from the active site through hydrophobic shielding or (ii) conferring a higher nucleophilic potential on the second substrate (homoserine) than water (*25*). The tunnel present in HTA could potentially function as a hydrophobic shield, but given the polar nature of the residues lining the wall of the tunnel, this strategy appears unlikely. Alternatively, examining the residues lining the wall of the tunnel suggests a mechanism by which the nucleophilic potential of homoserine could be increased over that of water. In addition to Ser143 and His337, Arg212 and Asp338 are also absolutely conserved. These residues are well positioned to interact with the carboxylic acid and primary amine moieties of homoserine, thereby positioning and steering the hydroxyl of the second substrate in the ideal location for acyl transfer from Ser143 (Figure 4). On the other hand, a water molecule would not be preferentially positioned at the location for optimal transfer of the acyl group, due to lack of stabilizing interactions.

CONCLUSION

Here we present the 1.65 Å resolution structure of HTA from *H. influenzae*. The structure identifies this enzyme to be a member of the α/β-hydrolase superfamily, possessing an additional lid domain with a novel fold. As such, this is the first example of an acetyltransferase enzyme structure having an α/β-hydrolase fold. Guided by previous kinetic and mutagenesis data, a detailed reaction mechanism can be proposed which explains the structural basis for the double displacement mechanism of HTA. Furthermore, the architecture of a tunnel provides a rationale of how HTA preferentially catalyzes acetyl transfer above hydrolysis. As HTA is a potential drug target for combating fungal and bacterial infections, the determination of the active site geometry and the identification of a nucleophilic serine have potential pharmaceutical application. This information allows for the development of inhibitors that alkylate Ser143, thereby obstructing Met biosynthesis. This strategy mirrors the approach taken by β-lactam antibiotics, which alkylate the nucleophilic serine of peptidoglycan transpeptidases.

ACKNOWLEDGMENT

The authors thank past and present members of the Berghuis and Wright laboratories for assistance and suggestions. We also thank Leon Flaks and Martin McMillan for assistance during data collection and financial support from CIHR and NSERC for operation of the X8C beamline.

REFERENCES

1. Umbarger, H. E. (1978) Amino acid biosynthesis and its regulation, *Annu. Rev. Biochem. 47*, 532−606.
2. Viola, R. E. (2001) The central enzymes of the aspartate family of amino acid biosynthesis, *Acc. Chem. Res. 34*, 339−349.
3. Yang, Z., Pascon, R. C., Alspaugh, A., Cox, G. M., and McCusker, J. H. (2002) Molecular and genetic analysis of the *Cryptococcus neoformans* MET3 gene and a met3 mutant, *Microbiology 148*, 2617−2625.
4. Jacques, S. L., Mirza, I. A., Ejim, L., Koteva, K., Hughes, D. W., Green, K., Kinach, R., Honek, J. F., Lai, H. K., Berghuis, A. M.,

and Wright, G. D. (2003) Enzyme-assisted suicide: molecular basis for the antifungal activity of 5-hydroxy-4-oxonorvaline by potent inhibition of homoserine dehydrogenase, *Chem. Biol. 10*, 989−995.
5. Arevalo-Rodriguez, M., Pan, X., Boeke, J. D., and Heitman, J. (2004) FKBP12 controls aspartate pathway flux in *Saccharomyces cerevisiae* to prevent toxic intermediate accumulation, *Eukaryotic Cell 3*, 1287−1296.
6. Bareich, D. C., Nazi, I., and Wright, G. D. (2003) Simultaneous in vitro assay of the first four enzymes in the fungal aspartate pathway identifies a new class of aspartate kinase inhibitor, *Chem. Biol. 10*, 967−973.
7. Ejim, L., Mirza, I. A., Capone, C., Nazi, I., Jenkins, S., Chee, G. L., Berghuis, A. M., and Wright, G. D. (2004) New phenolic inhibitors of yeast homoserine dehydrogenase, *Bioorg. Med. Chem. 12*, 3825−3830.
8. Hadfield, A., Kryger, G., Ouyang, J., Petsko, G. A., Ringe, D., and Viola, R. (1999) Structure of aspartate-beta-semialdehyde dehydrogenase from *Escherichia coli*, a key enzyme in the aspartate family of amino acid biosynthesis, *J. Mol. Biol. 289*, 991−1002.
9. DeLaBarre, B., Thompson, P. R., Wright, G. D., and Berghuis, A. M. (2000) Crystal structures of homoserine dehydrogenase suggest a novel catalytic mechanism for oxidoreductases, *Nat. Struct. Biol. 7*, 238−244.
10. Clausen, T., Huber, R., Prade, L., Wahl, M. C., and Messerschmidt, A. (1998) Crystal structure of *Escherichia coli* cystathionine gamma-synthase at 1.5 A resolution, *EMBO J. 17*, 6827−6838.
11. Clausen, T., Huber, R., Laber, B., Pohlenz, H. D., and Messerschmidt, A. (1996) Crystal structure of the pyridoxal-5′-phosphate dependent cystathionine beta-lyase from *Escherichia coli* at 1.83 Å, *J. Mol. Biol. 262*, 202−224.
12. Born, T. L., Franklin, M., and Blanchard, J. S. (2000) Enzyme-catalyzed acylation of homoserine: mechanistic characterization of the *Haemophilus influenzae* met2-encoded homoserine transacetylase, *Biochemistry 39*, 8556−8564.
13. Nazi, I., and Wright, G. D. (2005) Catalytic mechanism of fungal homoserine transacetylase, *Biochemistry 44*, 13560−13566.
14. Otwinowski, Z., and Minor, W. (1997) Processing of X-ray diffraction data collected in oscillation mode, in *Methods in Enzymology, Vol. 276: Macromolecular Crystallography* (Carter, C. W., Jr., and Sweet, R. M., Eds.) Part A, pp 307−326, Academic Press, New York.
15. Terwilliger, T. C. (2003) Automated main-chain model building by template matching and iterative fragment extension, *Acta Crystallogr., Sect. D: Biol. Crystallogr. 59*, 38−44.
16. Morris, R. J., Perrakis, A., and Lamzin, V. S. (2003) ARP/wARP and automatic interpretation of protein electron density maps, *Methods Enzymol. 374*, 229−244.
17. Murshudov, G. N., Vagin, A. A., Lebedev, A., Wilson, K. S., and Dodson, E. J. (1999) Efficient anisotropic refinement of macromolecular structures using FFT, *Acta Crystallogr., Sect. D: Biol. Crystallogr. 55* (Part 1), 247−255.
18. Janin, J. (1995) Principles of protein−protein recognition from structure to thermodynamics, *Biochimie 77*, 497−505.
19. Gibrat, J. F., Madej, T., and Bryant, S. H. (1996) Surprising similarities in structure comparison, *Curr. Opin. Struct. Biol. 6*, 377−385.
20. Heikinheimo, P., Goldman, A., Jeffries, C., and Ollis, D. L. (1999) Of barn owls and bankers: a lush variety of alpha/beta hydrolases, *Struct. Folding Des. 7*, R141−R146.
21. Ollis, D. L., Cheah, E., Cygler, M., Dijkstra, B., Frolow, F., Franken, S. M., Harel, M., Remington, S. J., Silman, I., Schrag, J., et al. (1992) The alpha/beta hydrolase fold, *Protein Eng. 5*, 197−211.
22. Nardini, M., and Dijkstra, B. W. (1999) Alpha/beta hydrolase fold enzymes: the family keeps growing, *Curr. Opin. Struct. Biol. 9*, 732−737.
23. Holmquist, M. (2000) Alpha/beta-hydrolase fold enzymes: structures, functions and mechanisms, *Curr. Protein Pept. Sci. 1*, 209−235.
24. Marchler-Bauer, A., Anderson, J. B., Cherukuri, P. F., DeWeese-Scott, C., Geer, L. Y., Gwadz, M., He, S., Hurwitz, D. I., Jackson, J. D., Ke, Z., Lanczycki, C. J., Liebert, C. A., Liu, C., Lu, F., Marchler, G. H., Mullokandov, M., Shoemaker, B. A., Simonyan, V., Song, J. S., Thiessen, P. A., Yamashita, R. A., Yin, J. J., Zhang, D., and Bryant, S. H. (2005) CDD: a conserved domain database for protein classification, *Nucleic Acids Res. 33*, D192−D196.
25. Milkowski, C., and Strack, D. (2004) Serine carboxypeptidase-like acyltransferases, *Phytochemistry 65*, 517−524.
26. Johnson, C. M., Roderick, S. L., and Cook, P. F. (2005) The serine acetyltransferase reaction: acetyl transfer from an acylpantothenyl donor to an alcohol, *Arch. Biochem. Biophys. 433*, 85−95.
27. DeLano, W. L. (2002) *The PyMOL Molecular Graphics System*, DeLano Scientific, San Carlos, CA.
28. Gilbert, D., Westhead, D., Viksna, J., and Thornton, J. (2001) A computer system to perform structure comparison using TOPS representations of protein structure, *Comput. Chem. 26*, 23−30.
29. Murzin, A. G., Brenner, S. E., Hubbard, T., and Chothia, C. (1995) SCOP: a structural classification of proteins database for the investigation of sequences and structures, *J. Mol. Biol. 247*, 536−540.
30. Beitz, E. (2000) TeXshade: shading and labeling of multiple sequence alignments using LaTeX2e, *Bioinformatics 16*, 135−139.
31. Sierk, M. L., and Kleywegt, G. J. (2004) Deja vu all over again: finding and analyzing protein structure similarities, *Structure (Camridge) 12*, 2103−2111.
32. Jeanmougin, F., Thompson, J. D., Gouy, M., Higgins, D. G., and Gibson, T. J. (1998) Multiple sequence alignment with Clustal X, *Trends Biochem. Sci. 23*, 403−405.
33. Gonnet, G. H., Cohen, M. A., and Benner, S. A. (1992) Exhaustive matching of the entire protein sequence database, *Science 256*, 1443−1445.

BI051951Y